Available online at www.sciencedirect.com
SCIENCE DIRECT®
Earth and Planetary Science Letters 222 (2004) 377–390
EPSL
www.elsevier.com/locate/epsl

# Strain softening and microstructural evolution of anorthite aggregates and quartz–anorthite layered composites deformed in torsion

Shaocheng Ji[a,d,*], Zhenting Jiang[b], Erik Rybacki[c], Richard Wirth[c], David Prior[b], Bin Xia[d]

[a] *Département des Génies Civil, Géologique et des Mines, École Polytechnique de Montréal, C.P. 6079, Succ. Centre-Ville, Montreal, QC, Canada H3C 3A7*
[b] *Department of Earth Sciences, University of Liverpool, L69 3BX, Liverpool, UK*
[c] *GeoForschungsZentrum Potsdam, D-14473 Potsdam, Germany*
[d] *Laboratory of Marginal Sea Geology, Guangzhou Institute of Geochemistry and South China Sea Institute of Oceanology, Chinese Academy of Sciences, Wushan, Guangzhou, PR China*

Received 20 November 2003; received in revised form 8 March 2004; accepted 15 March 2004

**Abstract**

Torsion experiments of anorthite (An) aggregates and layered composites with equal volume fractions of quartz (Qtz) and An were performed in a gas-medium apparatus at a confining pressure of 400 MPa, temperatures from 1373 to 1473 K, and twist rates from $1.0 \times 10^{-4}$ to $3.0 \times 10^{-4}$ rad/s. Dense specimens were fabricated from An glass and Qtz crystalline powder using hot isostatic pressing (HIP) techniques. Both An aggregates and Qtz–An layered composites show a continuous strain weakening from a peak stress at $\gamma = 0.2–0.3$ to $\gamma = 3.2$, and steady-state flow has not reached under the experimental conditions. The weakening is even more pronounced in the layered composites than the monolithic aggregates, suggesting channeling or localization of flow into the weak material between strong layers. The sheared An specimens developed pervasively C–S–C′ structures which are similar to those observed in natural ductile shear zones. TEM and electron backscattering diffraction (EBSD) fabric analyses suggest that grain boundary migration recrystallization-accommodated dislocation creep with (010)[100] as the dominant slip system was operating in the An. The strain softening may be due to the development of crystallographic preferred orientation (CPO), the operation of dynamic recrystallization and the formation of extremely fine-grained recrystallized material in the narrow C′ shear bands.


*Keywords:* anorthite; quartz–anorthite composite; simple shear; crystallographic preferred orientation; flow strength

## 1. Introduction

Plagioclase is the most abundant constituent in the continental and oceanic crust of the Earth [1]. It forms a continuous solid solution series ranging in composition from albite ($NaAlSi_3O_8$) to anorthite ($CaAl_2$

* Corresponding author. Tel.: +1-514-3404711x5134; fax: +1-514-3403970.
*E-mail address:* sji@polymtl.ca (S. Ji).

0012-821X/$ - see front matter © 2004 Elsevier B.V. All rights reserved.
doi:10.1016/j.epsl.2004.03.021

$Si_3O_8$). In this paper, we present our results on the rheological behaviour, microstructures and crystallographic preferred orientation (CPO) in monolithic anorthite (An) aggregates and layered composites with equal volume fractions of quartz (Qtz) and An, deformed in torsion at a confining pressure of 400 MPa and temperatures of 1373–1473 K. Three main considerations in undertaking this study were as follows.

(1) Tectonic deformation of the continental crust is mainly controlled by the rheological behaviour of the lower crust that is generally weaker than both the overlying upper crust and the underlying upper mantle [2–4]. To a first approximation, the rheology of the lower crust, in which plagioclase is volumetrically most important, can be taken to be the rheology of plagioclase [1–3]. Thus, an understanding of the evolution in microstructures and CPO of plagioclase deformed under well-defined conditions (*T*, *P*, stress and strain) is crucial to constraining the rheological behaviour of plagioclase. So far the interpretation of plagioclase's deformation and rheology in orogenic belts has been largely hindered by the relatively limited knowledge of mechanical and microstructural data from laboratory tests [5–14]. For example, the relative activity of different slip systems for plagioclase under varying physical and chemical conditions is still poorly known [10,14].
(2) Many ductile shear zones in high-grade metamorphic terranes that are representative of lower-crustal rocks were active under approximately simple shear (e.g., [15,16]). Almost all experimental deformation studies on feldspar in the ductile regime have been conducted in coaxial deformation tests [5–8,10,11]. In conventional, compression tests, strain is coaxial and the total axial strain is generally limited to less than 0.4, which corresponds to an equivalent shear strain of about 1. This amount of strain is usually insufficient to produce steady-state dislocation creep microstructures [17–20]. Application of experimental results obtained from coaxial compression to tectonic interpretation of ductile shear zones, where accumulated shear strains are often very large ($\gamma$>3), is thus limited. Also, in coaxial compression tests, progressive deformation results in a non-uniform stress state due to barrelling and/or buckling of the sample [20]. The so-called "diagonal saw-cut" experiments, using a sample wafer sandwiched between two rigid pistons cut at 30° or 45° [12,13] to their long axes, provide valuable information about non-coaxial deformation and its effects on microstructure and CPO evolution. However, this type of tests often involves a significant component of flattening across the shear zone and material extrusion into the gaps at the piston-cut edges. Thus, true simple shear deformation has not been produced in previous "diagonal saw-cut" experiments. In addition, the constraints brought into play by the lateral offsets of the split pistons may complicate the derivations of accurate strength data at high strains. However, simple shear deformation can be achieved in torsion experiments in the laboratory [9,17–20].
(3) CPO of plagioclase can further our understanding of its plastic deformation mechanisms, strain geometry, kinematics and deformation conditions, and enables us to evaluate its contribution to the seismic anisotropy of the lower crust. In spite of its importance, plagioclase has a much smaller CPO database than olivine, quartz and calcite. Reasons for this are primarily technical because plagioclase is triclinic. Full crystallographic orientations of plagioclase can be determined using the U-stage method [21,22] only across limited compositional ranges (An35–70 and An90–100) [23]. Conventional X-ray goniometry is not satisfactory for plagioclase CPO analysis due to the large number of overlapping diffraction peaks. Neutron diffraction goniometry has been applied to the measurements of plagioclase CPO [21,24]. However, relatively large volumes of sample material are required (>1 $cm^3$). Synchrotron X-ray goniometry was employed to investigate the CPO of albite aggregates [25], but this technique is expensive and not widely available. Recent studies [9,10,26,27] showed the most powerful technique for successfully measuring plagioclase CPO to be electron backscattering diffraction (EBSD) in a scanning electron microscope (SEM). We have used this new technique to collect representative plagioclase CPO data from our undeformed and deformed samples.

## 2. Samples

Commercial powders of anorthite ($An_{98.9}Or_{0.2}Ab_{0.9}$) glass with particle sizes ranging from 11 to 60 μm (Schott, Germany) and ground-up natural quartz with a grain size ranging from 20 to 80 μm (Johnson-Matthey, Germany) were used as the starting materials [10,11]. Four categories of samples were prepared using hot isostatic pressing (HIP) techniques. They are layered composites (LC, Fig. 1a), particulate composites (PC) of Qtz plus An, pure An (Fig. 1c) and pure Qtz aggregates. LC samples contain alternating Qtz and An layers with strong and sharp interfaces (Fig. 1b), which was created during cold pressing and subsequently thinned during HIP. The layering in cylindrical LC samples is characterized by the ratio of the diameter ($d$) to the thickness ($h$) of material layers. The PC is a homogeneous mixture with equal volume fractions of Qtz and An.

The An glass and Qtz powders were encapsulated in a steel jacket (diameter: 15 mm, length: 25 mm) and cold-pressed under an axial stress of about 150 MPa. Each cold-pressed pellet was HIPed in a Paterson gas-medium apparatus at 1123 K for 1 h, 1323 K for 1 h and then 1473 K for 3 h at a confining pressure of 300 MPa to maximize densification of the powder, to crystallize the glass, and to anneal the sample [8]. Porosity is $<1\%$ in the hot-pressed An and PC samples, 3–5% in the LC samples and 5–6% in the pure Qtz aggregates.

Under coaxial compression, the Qtz aggregates, in spite of their porosity of $\sim 5$–6%, do not yield at 1273–1373 K at confining pressure of 300 MPa and strain rate $10^{-5}$ $s^{-1}$ [10]. Even at 1473 K, the Qtz aggregate still has compressive strength higher than 600 MPa. Under the laboratory conditions (1473 K, 300 MPa and $10^{-5}$ $s^{-1}$), quartz is stronger than An by a factor of 40 (at $\varepsilon=0.15$) to 51 (at $\varepsilon=0.05$) [10].

From two typical HIPed samples from each category, several polished thin sections were made in order to characterize the microstructures and the water content of undeformed materials using optical, SEM, transmission electron microscope (TEM), Fourier transform infrared spectrometer (FTIR) and EBSD analyses.

The grain size ($D$) and aspect ratio ($S$) of a given grain were obtained from measuring its length ($L$) and ($W$) width from petrographic sections and SEM photographs of polished sections for Qtz and An, respectively. $D=\sqrt{LW}$ and $S=L/W$. Qtz displays a normal grain size distribution ranging from 15 to 80 μm with an arithmetic mean of 45 μm. The An grains display a log-normal size distribution ranging from 0.4 to 9 μm with an arithmetic average of 2.1

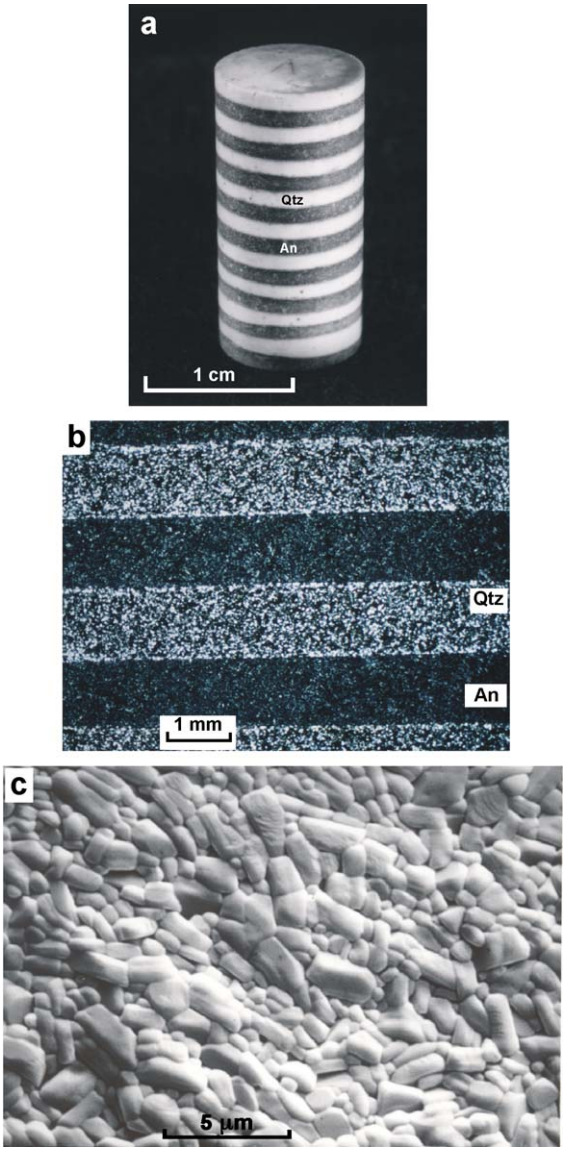


Fig. 1. Undeformed, hot isostatic pressed layered Qtz–An composite (a–b) and pure An aggregate (c). (a) Photograph, (b) optical photomicrograph, and (c) SEM micrograph. Sections of (b) and (c) were cut parallel to the cylinder axis.

μm. The mean aspect ratios for Qtz and An are 2.0 and 2.2, respectively. No discernable shape preferred orientation was observed for either Qtz or An in the HIPed samples.

Qtz in the PC aggregates forms large grains (15–80 μm) dispersed homogeneously within a continuous matrix of An. Spherulites with radial fibers of An are occasionally observed in pure An aggregates and An layers of LC samples and have sizes up to 60 μm. In the spherulites, anorthite fibers are generally tabular on {010} with an elongation mainly along [001] and to a lesser extent along [100]. However, no An spherulites occur in PC samples. It is generally accepted that spherulite texture results when the rate of crystal growth exceeds that of crystal nucleation [28]. Spherulites generally start from a nucleation centre where the water content is relatively high [11]. The volume fraction of spherulites in our An aggregates is about 10%.

TEM (Philips CM200, GFZ-Potsdam, Germany) operating at 200 kV shows that the grain boundaries in the An aggregates are coherent and high-angle. They are straight and clean, suggesting that the crystallization and compaction were well done. A small amount of melt ($\ll 0.5$ vol%) was observed in triple junctions. Anorthite grains in the HIPed samples are characterized by closely spaced growth twin lamellae and low dislocation densities ($\sim 10^{11}$ $m^{-2}$). The twins have their composition planes parallel to (010) and are mainly Albite, Carlsbad and Carlsbad-Albite types.

EBSD patterns of An and Qtz were measured and indexed using a SEM (Philips XL30) at Liverpool University, and the software package Channel+ from HKL Software Company [9,10,26,27]. The patterns were recorded at 30-kV acceleration voltage and nominal beam currents of 80 μA. No carbon coat was used on the thin sections, which were chemically–mechanically polished to remove specimen surface damage, because the coat degraded the EBSD image quality. In most cases, more than five or six bands were detected, allowing the bands to be indexed unambiguously by the computer simulation. The measurement uncertainty was given by the software as a mean angular deviation (MAD) between detected bands and simulated patterns. The indexing was not accepted if the MAD value was larger than 2°. EBSD measurements showed a random CPO of both An (Fig. 2) and Qtz in HIPed samples, as expected for hydrostatic conditions.

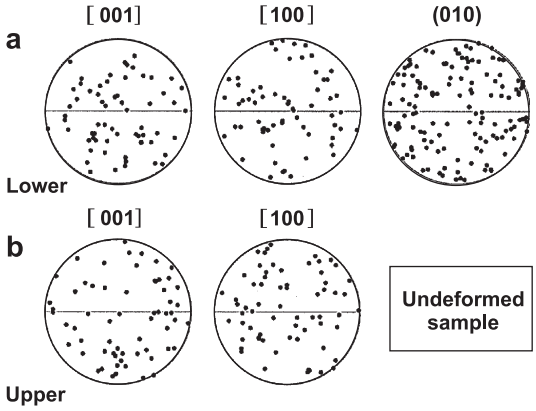


Fig. 2. Preferred orientations of triclinic anorthite [001], [100], and (010) for a undeformed, hot pressed, pure An aggregate. Notice that the whole sphere, rather than a hemisphere, is necessary to represent the distribution of the positive directions. Projections on the (a) lower and (b) upper hemispheres. Stereonets are equal-area plots; 130 measurements are used. The solid line is normal to the cylinder axis.

FTIR measurements using a Bruker IFS-66v (GFZ-Potsdam) showed a broad absorption band with a maximum near 3550 $cm^{-1}$ for HIPed samples. The spectra are typical for molecular water or hydroxyl [29]. The pure An samples and An layers from LC samples had a water content ranging from 8000 to 20000 H/$10^6$ Si with an average value of 13,000 H/$10^6$ Si ($\sim$ 0.08% wt.% $H_2O$). The pure Qtz samples and Qtz grains in PC samples contain very small amounts of water ($<$400 H/$10^6$ Si). There was no significant difference in water content of samples before and after experimental deformation because the samples were not vented. Thus, there was no detected loss of water species through the Fe jacket or the interface between the jacket and alumina pistons during the mechanical tests [11]. These water contents are lower than those found to produced diffusion creep [30].

## 3. Mechanical data

Torsion tests, which allow simple shear deformation with $\sigma_1 = -\sigma_3$ inclined at 45° to the axis of cylindrical samples [20], were carried out using a

Paterson-type gas-medium apparatus equipped with an internal torque cell (GFZ-Potsdam). The latter is able to apply torque to the specimen assembly with rates of twist over a range from $10^{-3}$–$10^{-7}$ rad/s. Both the sample and pistons were jacketed with iron sleeves with 0.23-mm wall thickness. The uncertainty in stress measurements falls within $\pm 5$ MPa. Temperature control was $\pm 3$ K along the gauge length of specimens. In the case of An aggregates and layered Qtz–An composites which are ductile above 1273 K, the total shear strains are limited mainly by the ductility of the Fe jacket.

All torsion tests were performed on cylindrical samples of 10-mm diameter and 10-mm length at a constant confining pressure of 400 MP, temperatures of 1373–1473 K, and constant twist rates ($\dot{\theta} = 1.0 \times 10^{-4}$ and $3.0 \times 10^{-4}$ rad/s). The principal mechanical data obtained in the torsion tests are torque $M$ versus time $t$ and twist $\theta$ versus time $t$. Fig. 3 shows typical torque–twist curves for pure An aggregates (Fig. 3a) and layered Qtz–An composites (Fig. 3b) at two different twist rates ($1.0 \times 10^{-4}$ and $3.0 \times 10^{-4}$ rad/s, corresponding to maximum shear strain rates of $5 \times 10^{-5}$ and $1.5 \times 10^{-4}$ $s^{-1}$ at the outer surface of the samples) and three different temperatures (1373, 1423 and 1473 K). The curves show that the shear strength of both An and LC samples is strongly influenced by twist rate and temperature, decreasing with an increase in temperature and a decrease in twist rate. The curves for An aggregates are characteristic of hot-working deformation: the torque (flow stress) increases rapidly up to a peak value at a relatively small plastic strain ($\theta = 20$–$30°$), then gradually decreases with increasing twist. Thus, steady-state flow of An has not been achieved up to a twist of 360° under the experimental conditions. Strain softening is more pronounced at higher temperature than at lower temperature (Fig. 3a).

In torsion tests of LC samples, the axis of rotation is perpendicular to the Qtz/An layering. Compared with the pure An aggregates, the LC samples display a similar shape of the torque–twist curves but with much more pronounced strain softening. The softening is interpreted as due to strong strain partitioning into weaker An layers while the Qtz layers remain practically undeformed. Comparison of Fig. 3a with Fig. 3b reveals that the peak shear strength of the LC samples is higher than that of the pure An aggregates.

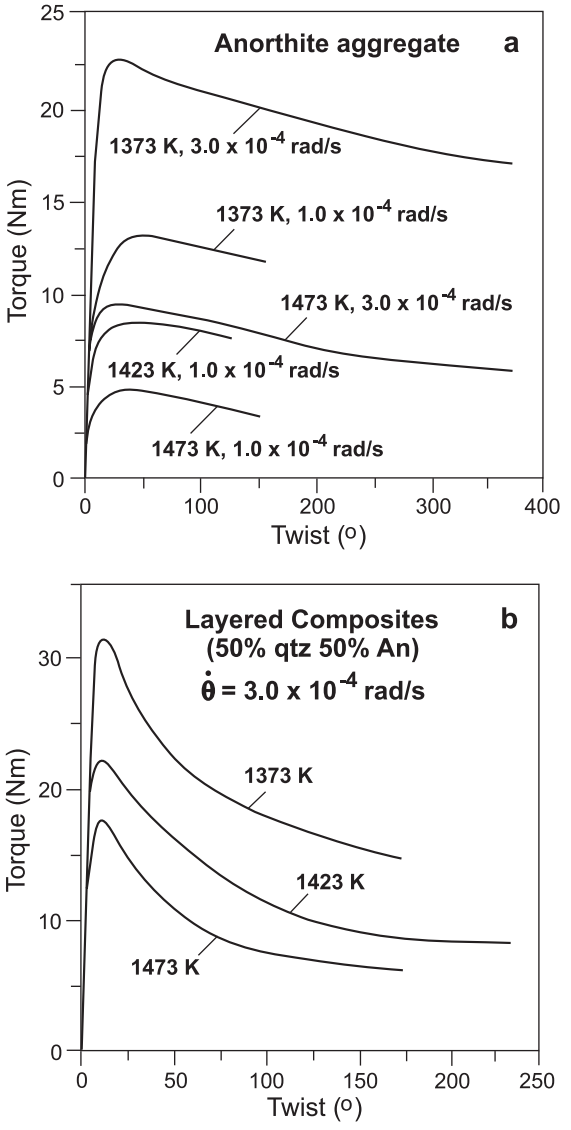


Fig. 3. Torque–twist curves for pure An aggregates (a) and Qtz–An layered composites (b) deformed by torsion at $P = 400$ MPa.

At a constant twist rate of $3 \times 10^{-4}$ rad/s, the maximum shear strength of LC samples is about 1.8 and 1.4 times higher than that of pure An aggregate at 1373 and 1473 K, respectively. At large strains ($\theta > 150°$), however, the LC samples become weaker than the pure An aggregates. At $\theta = 150°$ and a twist rate of $3 \times 10^{-4}$ rad/s, for instance, the shear flow strengths of the LC samples are only 82% and 76% of

those of the pure An aggregates at 1373 and 1473 K, respectively.

Six PC samples have been tested in torsion at temperatures of 1373–1523 K and twist rates of $10^{-4}$–$10^{-5}$ rad/s. However, slip occurred at the bottom sample–piston interface due to loss of frictional grip, and all tests failed. These LC samples could be too strong to be sheared in torsion under the experimental conditions.

## 4. Microstructures and CPO

The axial lines scribed on the outer surface of the Fe jacket of torsion specimens were used to indicate if heterogeneous strain took place during the tests. For all the twisted An aggregates, the scribe lines are straight and continuous, and the angle between the specimen axis and the scribe lines ($\phi$) was fairly constant along the length of the scribes, indicating uniform deformation on the bulk specimen scale. The latter reflects a homogeneous distribution of temperature along the sample assembly and no change in volume of the sample [20]. Furthermore, surface shear strain ($\gamma_s$) measurements using the scribe line angles and equation $\gamma_s = \tan\phi$ agreed with the values calculated based on the amount of twist and the specimen geometrical dimensions. In contrast to observations for the An aggregates, the scribe lines on the LC samples showed clear evidence of strong flow localization into the An layers. The scribe line of the An layers formed a large angle with the specimen axis while the line of the Qtz layers formed a very small angle with the specimen axis. This indicates that the weak An layers absorbed almost all the shear strain while the Qtz layers were almost rigid.

The sheared An specimens are characterized by C–S–C′ structures which developed pervasively over the sample scale (Figs. 4 and 5), and which are very similar to those observed in natural ductile shear zones [31,32]. The S plane (foliation) is defined by a strongly preferred alignment of An polycrystalline

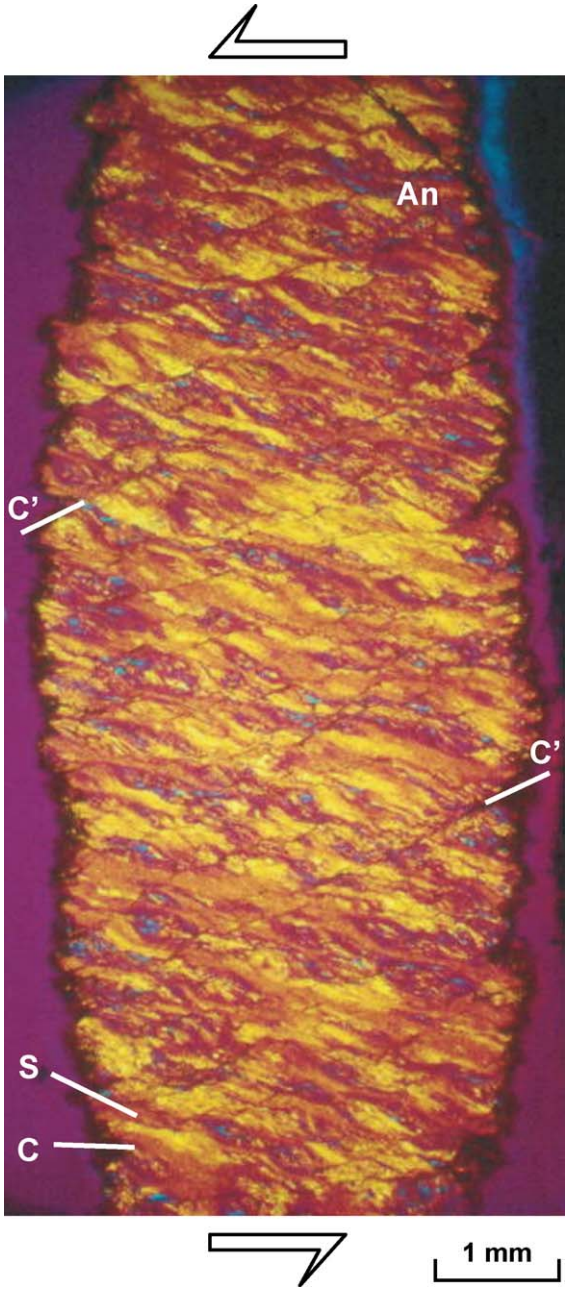


Fig. 4. Optical microstructure of a pure An aggregate deformed by torsion at $P=400$ MPa, $T=1373$ K, $\dot{\theta}=3.0\times10^{-4}$ rad/s and a maximum shear strain of 3.2. Crossed polarizers with an auxiliary gypsum plate. Foliation (S), boundary-parallel shear plane (C) and synthetic shear band (C′). The shear directions are indicated by semi-arrows. The different colors reflect different crystal axis orientations. The yellow grains have their (010) nearly parallel to the foliation and [100] subparallel to the stretching lineation. The blue grains, whose volume fraction is small (<5%), show distinct by different orientations, and are thus regarded as crystals with a hard orientation under the experimental conditions.

bands or ribbons. The latter display strong undulatory extinction, and contain smaller grains with apparently similar orientations (Fig. 4). C surfaces, which are parallel to the shear plane and perpendicular to the axis of torsion, are locally observed (Fig. 5a–b). In high strain parts near the outer surface of sheared samples, the polycrystalline bands are often obliterated by intense dynamic recrystallization, which significantly weakens the foliation (Fig. 5d). The angle ($\beta$) between the S and C planes varied with the shear strain ($\gamma$) and is generally smaller than the theoretical value calculated from $\gamma = 2\mathrm{ctg}(2\beta)$ [33]. C′ planes are en echelon arrays of synthetic shear zones, which are aligned about 15° to the boundary parallel shear plane C and dissect and offset the foliation S.

When the C surfaces are observed, the combination of the S and C planes defines sigmoidal or fish-shaped domains consistent with the imposed shear (Fig. 5a–b); the shear strain is more concentrated along the domain boundaries than the interior of the domains. The sigmoidal structures are strikingly similar to those commonly observed in natural shear zones [31,32]. The C′ planes represent a late disruption of an already developed foliation. It is also observed that the C′ planes become more closely spaced with increasing shear strain. At first glimpse, the C′ planes are fault-like features since they accommodate shear displacement as indicated by offset of markers such as the foliation. However, microscopic observations show these C′ planes are defined by very narrow zones of

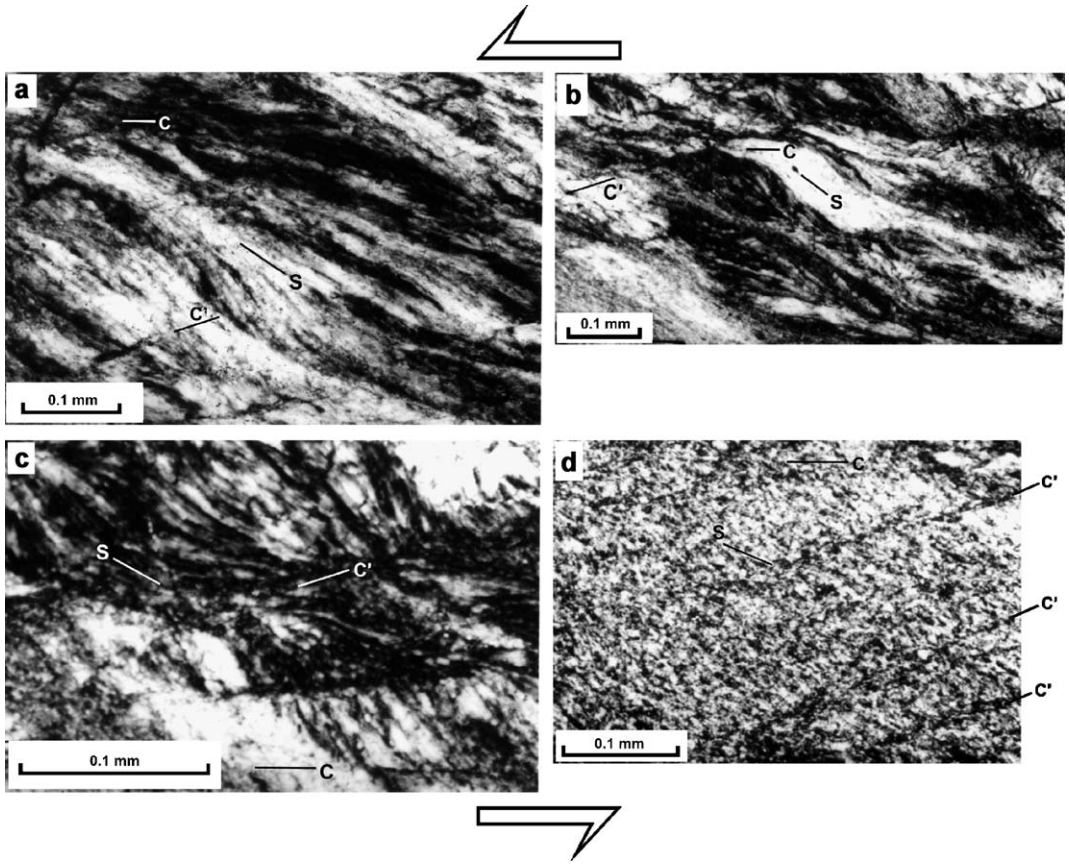


Fig. 5. Optical photomicrographs of pure An aggregates deformed by torsion. The sinistral shear sense is indicated by semi-arrows. (a) Sigmoidal foliation (S) curves towards the boundary-parallel shear plane (C), consistent with the sinistral sense of shear. (b) A fish-shaped domain bounded by the foliation (S) and the boundary-parallel shear plane (C) consistent with the sinistral sense of shear. (c) C′ shear bands are marked by narrow zones of recrystallized grains. (d) A completely recrystallized region ($\gamma = \sim 3.0$) where foliation is marked by individual elongated grains while the C′ plane is defined by narrow zones of extremely fine recrystallized grains.

extremely fine recrystallized grains. Thus, the physical properties of these deformation zones are actually not fault-like, and their mechanism is not one of frictional stick-slip deformation. Instead, the C′ shear is accomplished through a mechanism that involves strong strain concentration due to localized dynamic recrystallization.

It is observed, using cross polarizers with an auxiliary gypsum plate [5,6], that anorthite grains have a relatively uniform color except some porphyroclasts (Fig. 4). These porphyroclasts are unfavourably oriented with respect to the imposed shear and hence remain as weakly deformed augen [15]. The uniform color in the rest of the sample indicates a strong CPO.

Because each sample deformed by torsion shows a gradient of strain from the centre of rotation to the outer edge of the sample, we calibrated the CPO variation as a function of shear strain using a single sample that deformed under the same $T$ and $P$ conditions. The CPO of An from a pure An aggregate achieved a maximum shear strain of 3.2 at 1473 K and a twist rate of $3.0 \times 10^{-4}$ rad/s was measured using the EBSD technique. Although grid measurements with 40-μm spacing were made across the thin sections, the recrystallized grains and particularly those within the C′ shear bands are too small to be measured. The CPO diagrams shown in Fig. 6 are thus representative of the fabrics of the coarse porphyroclasts. The (010) poles and [100] directions developed an obvious preferred orientation close, respectively, to the normal to the foliation and to the stretching lineation. The CPO strength increases first rapidly from $\gamma = 0$ to $\gamma = 1$ and then increases slowly with shear strain up to $\gamma = 3$.

Similar to An samples deformed by coaxial compression [10] at the same conditions, the An aggregates or layers deformed by torsion exhibit TEM microstructures indicative of dislocation creep accommodated by grain boundary migration recrystallization. The An grains display variable dislocation densities with very high densities ($>5 \times 10^{14}$ $m^{-2}$) in relict grains and very low densities ($5-8 \times 10^{11}$ $m^{-2}$ in recrystallized neograins (Fig. 7). Even within the grains with very high dislocation densities, the distribution of dislocations is heterogeneous, with dislocations clustered along narrow planar zones that are generally parallel to (010) planes. The planar

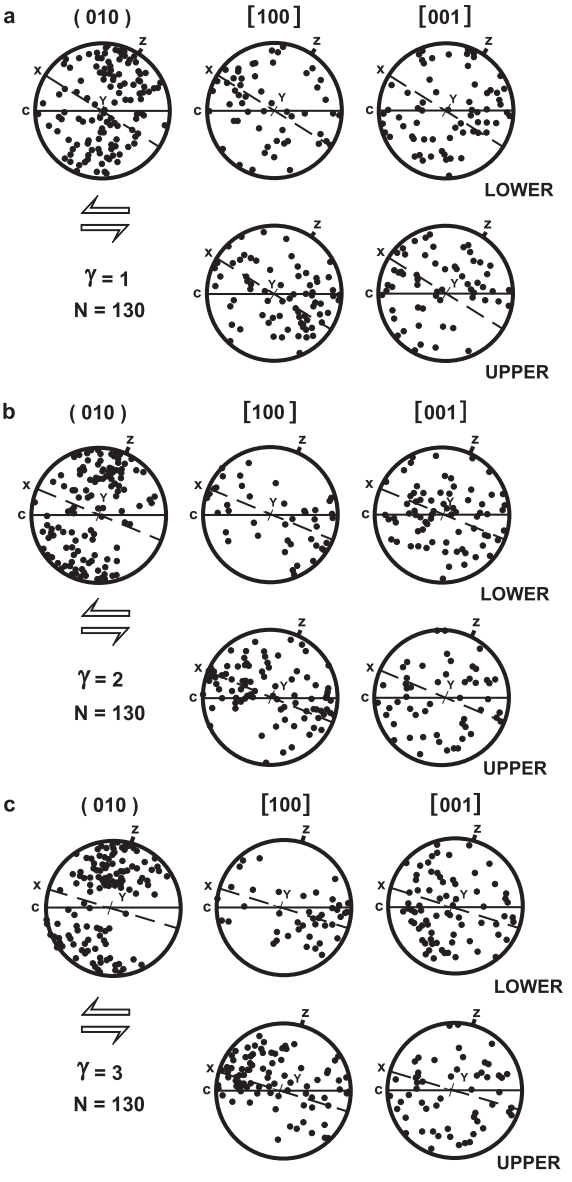


Fig. 6. Crystallographic preferred orientations of anorthite porphyroclasts from a pure An aggregate deformed by torsion at $P = 400$ MPa, $T = 1473$ K, $\dot{\theta} = 3.0 \times 10^{-4}$ rad/s and three different shear strains: $\gamma = 1$ (a), $\gamma = 2$ (b), and $\gamma = 3$ (c). C is the boundary-parallel shear plane (horizontal line); X is parallel to the stretching lineation; Z is the normal to the foliation (XY-plane). Notice that the whole sphere, rather than a hemisphere, is necessary to represent the distribution of the positive directions. [100] and [001] are projected on the upper and lower hemispheres while the poles to (010) are plotted on the lower hemisphere. Stereonets are equal-area plots. One hundred thirty measurements are used.

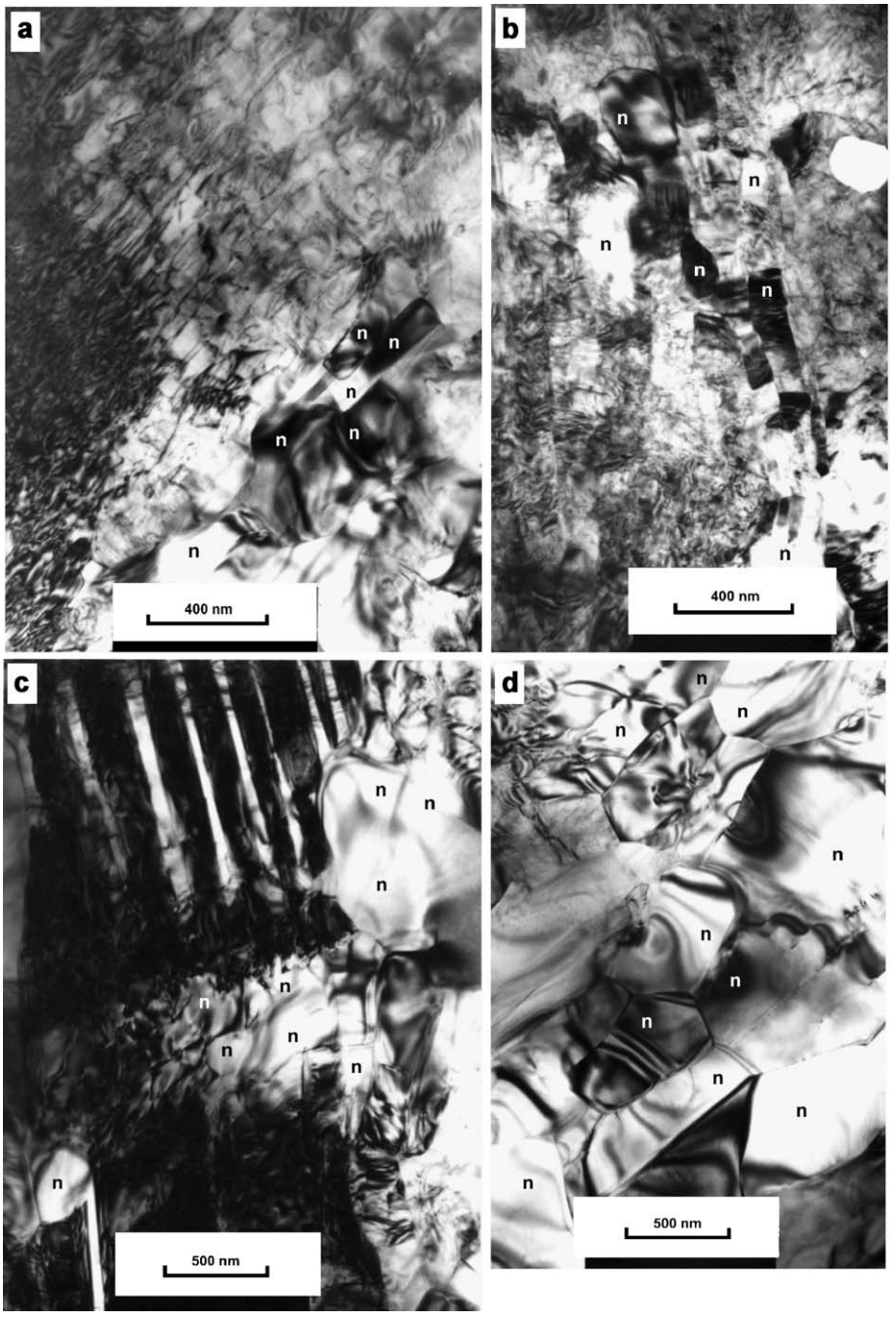


Fig. 7. TEM (bright field) micrographs showing typical substructures of dislocations and dynamic recrystallization in anorthite deformed by torsion at $P=400$ MPa, $T=1473$ K, $\dot{\theta}=3.0\times10^{-4}$ rad/s. The distribution of dislocations is heterogeneous and grain boundary migration toward highly strained grains with very high (tangled) dislocation density forms recrystallized grains (*n*). (a), (b) and (d) from a pure anorthite aggregate; (c) from an anorthite layer in a layered Qtz–An sample; (d) from a C′ shear zone.

zones of high dislocation density indicate that the (010) plane is the main slip plane under the conditions of investigation. Furthermore, the deformed An developed strongly sutured grain boundaries with neograins bulging from regions with very high dislocation densities to areas with low dislocation densities (Fig. 7c). No well-developed subgrain boundaries or dislocation walls have been observed. The microstructure is similar to those typically observed in plagioclase deformed at moderate and high temperatures [1,5–7,10,16,22,34].

## 5. Discussion

### 5.1. CPO

Anorthite grains show a random CPO in undeformed, HIPed aggregates (Fig. 2). In both An aggregates and LC samples deformed by torsion, however, anorthite grains develop a strong CPO with the poles to (010) rotated progressively to align parallel to the foliation plane and the [100] axes tending to lie in the foliation plane with the maximum concentration parallel to the stretching lineation (Fig. 6). Thus, the CPO formed during the torsion rather than from the HIP, and provided evidence for the dominance of dislocation creep. Numerical models of simple shear [35,36], in which only one slip system is available to each grain, predict that the slip plane and the slip direction align progressively close to the shear plane and shear direction, respectively, with increasing shear strain. Thus, the CPO pattern observed from the sheared An aggregates is consistent with dislocation motion on (010)[100] system, supporting that it is the easiest slip system under the experimental conditions. The results agree with our previous CPO measurements of An aggregates deformed in coaxial compression at high temperature where the porphyroclasts developed a strong CPO with the poles to (010) parallel to $\sigma_1$ and a girdle of [100] normal to $\sigma_1$ [10]. As shown in Fig. 6, the An fabric strength increases nonlinearly with increasing shear strain; a rapid increase occurs up to $\gamma = 1$ and then a relatively slow further increase between $\gamma = 1$ and $\gamma = 3$ at the same twist rate ($3.0 \times 10^{-4}$ rad/s). This trend could be caused by the onset of grain boundary migration recrystallization and development of C′ shear bands at $\gamma > 1$ because these processes made the strain preferentially partitioned into the shear zones and left the rest of the sample less deformed. Due to the lack of models for CPO development and evolution with strain in triclinic plagioclase using a relaxed Taylor theory or the viscoplastic self-consistent theory [37,38], a more quantitative interpretation of the CPO pattern and strength is impossible at this time.

In anorthite, the strongest bonds are the Al–O and Si–O tetrahedral or T–O bonds. The easiest glide planes will be those intersecting the smallest number of T–O bonds per unit area. Using this criterion, the easiest glide planes in anorthite should be (010) with two T–O bonds per unit cell, followed by (001), (110), ($\bar{1}\bar{1}0$) and ($10\bar{1}$) with four each, and then (100) and (111) with six [1,15]. The easiest slip direction will have the shortest Burgers vector because these dislocations have the lowest energy and are the most stable. If we restrict ourselves to possible Burgers vectors in the easiest glide plane (010), then we would expect 1/2[001] with $\vec{b} = 0.7$ nm which is dissociated and [100] with $\vec{b} = 0.8$ nm. It has been observed that c-slip on (010) planes is dominant in plagioclase in natural mylonites of upper amphibolite and granulite facies [14–16,22–24,34] while a-slip on (010) or (001) planes is dominant in experimentally deformed mafic plagioclase [10,39]. Thus, a transition from dominantly c-slip to a-slip may occur in plagioclase with increasing temperature, strain rate and/or $H_2O$ content, and decreasing confining pressure.

In triclinic anorthite, there are certainly not enough independent slip systems to produce either homogeneous or arbitrary deformation in a polycrystalline sample. Many features in our sheared samples such as inhomogeneous dislocation density and grain boundary migration recrystallization all indicate heterogeneous strain. High densities of dislocations result from interaction between dominant (010)[100] system and other secondary slip systems such as (010)[001], (010)[101], (001) [100] and (110)[001]. If just one dominant slip system and a few secondary slip systems can be activated, strain will lead to lattice rotation and rapidly form strong CPO. The texture analysis suggests that anorthite deforms largely by slip on just one dominant system, (010)[100], while grain boundary migration recrystallization plays a role in relieving the strain incompatibilities which would

otherwise result from such limited slip systems. It remains unclear if submicron-sized neograins in the C′ shear bands develop a CPO because they are too small to measure with EBSD.

### 5.2. Flow strength

Our study allows us to relate microstructures to mechanical properties. For example, the significant strain softening in pure An aggregates, which should involve a change in deformation microstructure, appears to be associated with the formation of C′ shear bands and the operation of dynamic recrystallization. The An samples contain ~0.08 wt.% water; half of it may be stored in the crystals [40] while another half at the grain boundaries. The latter may have diffused into C′ shear bands during shear, just like the melt segregated from olivine-basalt aggregates deformed in shear into channels aligned synthetically at 15–20° to the shear boundary [41]. The diffusion of water into the C′ shear bands leads to dynamic recrystallization and hydrolytic weakening. Since the spot size of the FTIR microscope is about 20 times larger than the average anorthite grain size, it was impossible for us to quantify the relative concentration of water in the C′ shear bands with respect to the rest of the samples. Moreover, grain boundary sliding in the extremely fine recrystallized grains may also make some contribution to the softening. The submicron-sized neograins possess a much larger fraction of atoms at grain boundaries than larger original grains. The plastic deformation localized in the C′ zones may be caused by a large number of small sliding events of atomic planes at the grain boundaries, with only a minor part being caused by dislocation activity in the grains. Recrystallization as a mechanism of strain weakening in the regime of dislocation creep has been documented in experimentally deformed albite [1,5–7] and naturally deformed plagioclase (e.g., [16,34]). We reproduced for the first time recrystallization-induced strain softening in simple-sheared anorthite using a gas-medium apparatus with high precisions in mechanical data.

Quartz is rheologically stronger than anorthite under laboratory conditions. In natural felsic mylonites deformed at greenschist to amphibolite grade, however, quartz is generally weaker than feldspar. It is well known that the relative strength contrast between two mineralic phases may change with deformation conditions such as temperature, strain rate, water content, strain path and operative deformation mechanism (see [10] for discussion). The main objective of this study is to reveal some fundamental principles in the rheology of polyphase rocks. For example, layered samples with equal volume fractions of Qtz and An have a higher peak strength than the pure An aggregates at low shear strain, but the flow stress for the first becomes lower than the latter at high shear strains. Layered samples display a greater degree of strain weakening than pure weak-phase aggregates. The observed dramatic weakening for the layered composites under layer-parallel shear offers an important piece of evidence supporting channel flow of weak materials between strong layers, which is expected to prevail in the deep continental crust [4]. Our results also provide a reasonable explanation for localized deformation in layered polyphase rocks.

### 5.3. Microstructures

The foliation (S) is dragged by the C′ shear bands, indicating that the latter formed after the first. This fact is consistent with the suggestion of Platt and Vissers [42] from field observations of mylonites. According to these authors, the foliation rotates progressively towards the shear zone boundary (C) with increasing shear. When the angle between S and C reaches a small value then shear is able to occur in part along the S plane. This shear component results in the onset of dynamic recrystallization in a series of narrow shear zones (C′) at about 15° to the C plane; the C′ planes are synthetic relative to the sense of overall shear. Hence, the S–C′ structure is a reliable shear sense indicator.

Fig. 8 shows a typical structure in granulite facies anorthositic mylonites from the Jotun Nappe in southern Norway. The mylonites consist of plagioclase (55–85%, An40–50), clinopyroxene and amphibole (14–40%) and garnet (3–10%). The S plane is remarked by strongly elongate plagioclase porphyroclasts that show clear evidence of intracrystalline plastic deformation such as undulatory extinction, deformation bands, kink band and serrated boundaries. The C′ planes are defined by narrow zones of very fine recrystallized grains. The ribbon porphyr-

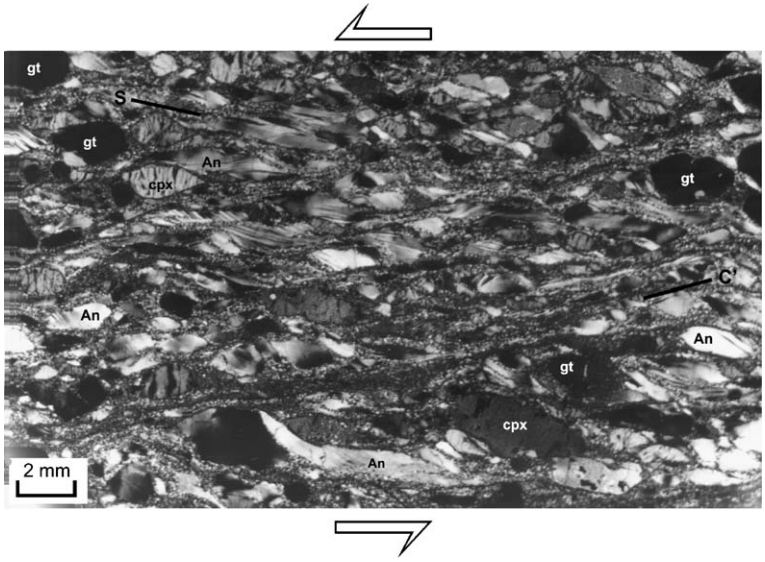


Fig. 8. S–C′ structure of an anorthosite mylonite from a granulite-facies shear zone in the Jotun nappe complex, Jotunheimen, Norway. The S foliation (S) is defined by elongate plagioclase porphyroclasts, whereas the C′ shear bands are defined by a set of parallel microshear zones composed of fine recrystallized grains. The sinistral shear sense is indicated by semi-arrows. XZ section, crossed polarizers. Optical and TEM microstructures and CPO data were reported in previous papers [22,34].

oclasts have their tapering ends rotated into parallelism with the C′ planes. The C′ planes obviously formed after the initial foliation. Ductile strains tend to be concentrated along the C′ planes because fine recrystallized grains are weak [5–7]. The similarities of these natural mylonites [15,16,22,34] and our experimentally sheared samples are striking in terms of both S–C′ structure and recrystallization, although the dominant slip system inferred from the CPO is (010)[001] in the natural mylonites while (010)[100] in the experimentally sheared samples. The S–C′ structure in feldspar-rich rocks should receive renewed interpretation with the view that strain softening is induced by water segregation and dynamic recrystallization localized into the C′ planes.

## 6. Conclusions

The plasticity and strain softening of An aggregates and layered composites containing equal volume fractions of Qtz and An were investigated by torsion tests at temperatures of 1373–1473 K, a confining pressure of 400 MPa and twist rates of $1.0\times10^{-4}$–$3.0\times10^{-4}$ rad/s. Both the An aggregates and the Qtz–An layered composites show a continuous strain weakening after a peak stress at a shear strain of about 0.2–0.3, and no steady-state is reached before $\gamma = \sim 3$. The weakening is more pronounced in the layered composites than in the monolithic aggregates, indicating the channel flow of the weak material between strong layers. Furthermore, the sheared An aggregates developed pervasive C–S–C′ microstructures similar to those observed in natural ductile shear zones. TEM observations of the anorthite indicate that the dominant deformation mechanism was dislocation creep accommodated by grain boundary migration recrystallization. The anorthite porphyroclasts develop a strong CPO with the (010) plane parallel or subparallel to the foliation and the [100] direction is aligned parallel or subparallel to the stretching lineation. This pattern indicates that (010) is the easiest slip plane and that [100] slip is easier than [001] slip for our experimental conditions. The observed strain softening in anorthite is due to the operation of dynamic recrystallization by grain boundary migration [5–7], the development of the crystallographic preferred orientation, and strain localization into the extremely fine-grained recrystallized material along the narrow C′ shear zones.

## Acknowledgements

This study was supported by NSERC of Canada, the Alexander von Humbodt Foundation of Germany, and Guangzhou Institute of Geochemistry, Chinese Academy of Sciences. We thank S. King, T. Tharp, J. Tullis, M.E. Zimmerman for the comments and suggestions. We are indebted to G. Dresen, A. Dimanov, M.S. Paterson and J. Wheeler for the helpful discussion, Michel Naumann for the technical assistance with the high *T* and *P* experiments, Stefan Gehrmann for the preparation of thin sections, and André Lacombe for drawing the figures. This is LITHOPROBE contribution no. 1362. ***[SK]***

## References

[1] J. Tullis, Experimental studies of deformation mechanisms and microstructures in quartzo-feldspathic rocks, in: D.J. Barber, P.G. Meredith (Ed.), Deformation Processes in Minerals, Ceramics and Rocks, Unwin Hyman, London, 1990, pp. 190–227.

[2] G. Ranalli, Rheology of the Earth, Chapman & Hall, London, 1995, 413 pp.

[3] S.C. Ji, B. Xia, Rheology of Polyphase Earth Materials, Polytechnic International Press, Montreal, Canada, 2002, 259 pp.

[4] C. Beaumont, R.A. Jamieson, M.H. Nguyen, B. Lee, Himalayan tectonics explained by extrusion of a low-viscosity crustal channel coupled to focused surface denudation, Nature 414 (2001) 738–742.

[5] J. Tullis, R. Yund, Dynamic recrystallization of feldspar: a mechanism for ductile shear zone deformation, Geology 13 (1985) 238–241.

[6] J. Tullis, L. Dell'Angelo, R. Yund, Ductile shear zones from brittle precursors in feldspathic rocks: the role of dynamic recrystallization, in: A. Duba, W. Durham, J. Handin, H. Wang (Eds.), The Brittle–Ductile Transition, The Heard Volume, Am. Geophys. Union Monogr. 56 (1990) 67–82.

[7] S.C. Ji, D. Mainprice, Experimental deformation of sintered plagioclase above and below the order–disorder transition, Géodin. Acta 1 (1987) 113–124.

[8] A. Dimanov, G. Dresen, X. Xiao, R. Wirth, Grain boundary diffusion creep of synthetic anorthite aggregates: the effect of water, J. Geophys. Res. 104 (1999) 10483–10497.

[9] S.C. Ji, Z. Jiang, R. Wirth, Crystallographic preferred orientation (CPO) of experimentally sheared plagioclase aggregates: implications for crustal heterogeneity (abstract), EOS Trans.-Am. Geophys. Union 80 (1999) 916.

[10] S.C. Ji, R. Wirth, E. Rybacki, Z. Jiang, High-temperature plastic deformation of quartz–plagioclase multilayers by layer-normal compression, J. Geophys. Res. 105 (2000) 16651–16664.

[11] E. Rybacki, G. Dresen, Dislocation and diffusion creep of synthetic anorthite aggregates, J. Geophys. Res. 105 (2000) 26017–26036.

[12] A. Post, J. Tullis, A recrystallized grain size piezometer for experimentally deformed feldspar aggregates, Tectonophysics 303 (1999) 159–173.

[13] H. Stunitz, J. Tullis, Weakening and strain localization produced by syn-deformational reaction of plagioclase, Int. J. Earth Sci. 90 (2001) 136–148.

[14] H. Stünitz, J.D. Fitz Gerald, J. Tullis, Dislocation generation, slip systems and dynamic recrystallization in experimentally deformed plagioclase single crystals, Tectonophysics 372 (2003) 215–233.

[15] S.C. Ji, D. Mainprice, F. Boudier, Sense of shear in high-temperature movement zones from the fabric asymmetry of plagioclase feldspars, J. Struct. Geol. 10 (1988) 73–81.

[16] R. Kruse, H. Stünitz, K. Kunze, Dynamic recrystallization processes in plagioclase porphyroclasts, J. Struct. Geol. 23 (2001) 1781–1802.

[17] M. Bystricky, K. Kunze, L. Burlini, J.P. Burg, High shear strain of olivine aggregates: rheological and seismic consequences, Science 290 (2000) 1564–1567.

[18] M. Pieri, L. Burlini, K. Kunze, I. Stretton, D. Olgaard, Rheological and microstructural evolution of Carrara marble with high shear strain: results from high temperature torsion experiments, J. Struct. Geol. 23 (2001) 1393–1413.

[19] E. Rybacki, M.S. Paterson, R. Wirth, G. Dresen, Rheology of calcite–quartz aggregates deformed to large strain in torsion, J. Geophys. Res. 108 (2003) 2089 (doi: 10.1029/2002JB001833).

[20] M.S. Paterson, D.L. Olgaard, Rock deformation tests to large shear strains in torsion, J. Struct. Geol. 22 (2000) 1341–1358.

[21] H.R. Wenk, H.J. Bunge, E. Jansen, J. Pannetier, Preferred orientation of plagioclase: neutron diffraction and U-stage data, Tectonophysics 126 (1986) 271–284.

[22] S. Ji, D. Mainprice, Natural deformation fabrics of plagioclase: implications for slip systems and seismic anisotropy, Tectonophysics 147 (1988) 145–163.

[23] S.C. Ji, X. Zhao, P. Zhao, On the measurement of plagioclase petrofabric, J. Struct. Geol. 16 (1994) 1711–1718.

[24] Y.X. Xie, H.R. Wenk, S. Matthies, Plagioclase preferred orientation by TOF neutron diffraction and SEM-EBSD, Tectonophysics 370 (2003) 269–286.

[25] F. Heidelbach, A. Post, J. Tullis, Crystallographic preferred orientation in albite samples deformed experimentally by dislocation and solution precipitation creep, J. Struct. Geol. 22 (2000) 1649–1661.

[26] D. Prior, J. Wheeler, Feldspar fabrics in a greenschist facies albite-rich mylonite from electron backscatter diffraction, Tectonophysics 303 (1999) 29–49.

[27] Z.T. Jiang, D.J. Prior, J. Wheeler, Albite crystallographic preferred orientation and grain misorientation distribution in a low-grade mylonite: implications for granular flow, J. Struct. Geol. 22 (2000) 1663–1674.

[28] A. Spry, Metamorphic Textures, Pergamon, New York, 1983, 352 pp.

[29] R.D. Aines, G.R. Rossman, Water in minerals? J. Geophys. Res. 89 (1984) 4059–4071.

[30] J. Tullis, R.A. Yund, J. Farver, Deformation-enhanced fluid distribution in feldspar aggregates and implications for ductile shear zones, Geology 24 (1996) 63–66.
[31] D. Berthe, P. Choukroune, P. Jegouzo, Orthogneiss, mylonite and non-coaxial deformation of granites: the example of the South Armorican Shear Zone, J. Struct. Geol. 1 (1979) 31–42.
[32] A.W. Snoke, J. Tullis, V.R. Todd, Fault-Related Rocks: A Photographic Atlas, Princeton Univ. Press, New Jersey, 1998, 617 pp.
[33] J.G. Ramsay, M.I. Huber, The Techniques of Modern Structural Geology, Vol. 1: Strain Analysis, Academic Press, London, 1983, 307 pp.
[34] S.C. Ji, D. Mainprice, Recrystallization and fabric development in plagioclase, J. Geol. 98 (1990) 65–79.
[35] A. Etchecopar, A plane kinematic model of previous deformation in a polycrystalline aggregate, Tectonophysics 39 (1977) 121–139.
[36] A. Etchecopar, G. Vasseur, A 3-D kinematic model of fabric development in polycrystalline aggregates: a comparison with experimental and natural examples, J. Struct. Geol. 9 (1987) 705–717.
[37] H.R. Wenk, C.N. Tomé, Modeling dynamic recrystallization of olivine aggregates deformed in simple shear, J. Geophys. Res. 104 (1999) 25513–25527.
[38] A. Tommasi, D. Mainprice, G. Canova, Y. Chastel, Viscoplastic self-consistent and equilibrium-based modeling of olivine lattice preferred orientations: implications for the upper mantle anisotropy, J. Geophys. Res. 105 (2000) 7893–7908.
[39] M.E. Zimmerman, D.L. Kohlstedt, Melt segregation and LPO in anorthite-basalt deformed in torsion, Eos, Trans.-Am. Geophys. Union, Fall Meet. Suppl., Abstract 84 (2003) F1045.
[40] H. Behrens, Structural, kinetic and thermodynamic properties of hydrogen in feldspar, Kinetic Processes in Minerals and Ceramics, EFS Workshop on Cation Ordering, Eur. Sci. Found., Cambridge, UK, 1994, pp. 1–7.
[41] D.L. Kohlstedt, M.E. Zimmerman, Rheology of partially molten mantle rocks, Annu. Rev. Earth Planet. Sci. 24 (1996) 41–62.
[42] J.P. Platt, R.L.M. Vissers, Extensional structures in anisotropic rocks, J. Struct. Geol. 2 (1980) 397–410.